Paper 269

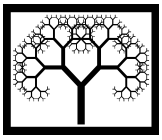

Proceedings of the Eleventh International Conference
on Computational Structures Technology,
B.H.V. Topping, (Editor),
Civil-Comp Press, Stirlingshire, Scotland

Shakedown Analysis in *n*-dimensional Loading Spaces with Kinematical Hardening

J.-W. Simon
Institute of Applied Mechanics
RWTH Aachen University, Germany

Abstract

The load bearing capacity of engineering structures subjected to varying thermo-mechanical loading can be determined most conveniently by shakedown analysis. Admittedly, if kinematical hardening is considered, shakedown analysis is, as yet, restricted to either one or two independently varying loads. In consequence, the aim of this paper is to extend existing formulations for arbitrary numbers of loading, which is inevitable for most technical applications. For this, limited kinematical hardening was incorporated into MELAN's shakedown theorem by means of a two-surface model covering both alternating plasticity and ratcheting, generalized to n-dimensional loading spaces. As a result, the first three-dimensional shakedown domain accounting for hardening is presented for a flanged pipe subjected to thermo-mechanical loading.

Keywords: shakedown analysis, n-dimensional loading space, limited kinematical hardening, interior-point algorithm, convex optimization, nonlinear programming.

1 Introduction

Determining the load bearing capacity is essential for the design of engineering structures, but poses a challenging task in case of varying thermo-mechanical loading beyond the elastic limit. In general, if the loading varies with time, the limit state of the considered elasto-plastic structure is defined by: instantaneous collapse, alternating plasticity, or incremental collapse –often referred to as ratcheting in the case of cyclic loading. However, if none of these failure mechanisms occur, the system is designated "safe" and the corresponding maximum loading factor is denoted by α_{SD}.

Ascertaining α_{SD} by means of the conventional step-by-step methods, where the loading path is divided into small time steps entailing a full analysis of stresses and strains in each step, generally leads to cumbersome computations. Moreover, the

whole loading history needs to be given deterministically, which is not realistic in many technical applications. Alternatively, direct methods –comprising limit and shakedown analysis– are appropriate to avoid these problems, see e.g. [1–3], because they do not require the exact loading history but only its bounding envelope. Therefore, in this paper, direct methods are applied to determine the shakedown factor.

In particular, the static approach by MELAN [4, 5] is adopted, which gives a lower bound to the shakedown factor, and thus leads to conservative solutions in principle. Originally, MELAN's theorem has been formulated for elastic-perfectly plastic and for unlimited kinematical hardening continua. Since incorporating only unlimited kinematical hardening does not cover incremental collapse but solely alternating plasticity, see e.g. [6–8], this is inadequate to realistically reflect the behavior of most engineering structures. Hence, taking into account limited kinematical hardening is important for obtaining realistic results.

The first explicit formulation for limited kinematical hardening materials was given by WEICHERT and GROSS-WEEGE [9, 10], who introduced a two-surface model, followed by STEIN et al. [11, 12]. Later, HEITZER [13] showed that these formulations can be transferred one to the other.

Since the lower bound theorem is formulated in statical quantities, it is particularly suited for introducing limited kinematical hardening with the two-surface model, see e.g. [14–16]. On the other hand, it leads to nonlinear convex optimization problems, which are typically characterized by large numbers of unknowns and constraints when considering problems of practical relevance. From the different techniques to solve such problems, the interior-point method exhibits a high potential especially for large-scale problems, see e.g. [17, 18]. Although several powerful interior-point based solvers exist –such as IPOPT [19, 20], KNITRO [21, 22], and LOQO [23, 24]– these are designed to solve a preferably wide variety of problems, accepting less efficient performance compared to problem-tailored codes. The same holds for the program MOSEK [25, 26] designed for second order conic problems, which gained importance in the field of limit and shakedown analysis in recent years, see e.g. [27–30].

However, for efficiency reasons, a number of alternative interior-point algorithms were presented, e.g. [31–40], which especially adapted the solution strategy to the underlying problem. Among these, the algorithm IPDCA was invented for VON MISES-type materials, which allowed for application to large-scale engineering problems, see [35, 36]. More recently, predicated on IPDCA, the new interior-point algorithm IPSA was developed, being distinguished by a particularly problem-oriented solution strategy [41, 42]. Whereas both IPDCA and the original formulation of IPSA were restricted to elastic-perfectly plastic materials, the latter was extended to take into account limited kinematical hardening [43].

Notably, up to now, IPSA is the only algorithm capable of solving shakedown problems with multi-dimensional loading spaces, see [44], such that arbitrary numbers of loadings can be considered. As yet, this is only available for elastic-perfectly plastic materials. In consequence, an extension is presented in this paper, incorporating both limited kinematical hardening material behavior and n-dimensional loading spaces.

The paper is organized as follows: The background of lower bound shakedown analysis for elastic-perfectly plastic materials is summarized in Section 2, already including arbitrary numbers of loadings. In Section 3, the limited kinematical hardening behavior is incorporated using a two-surface model. Section 4 is dedicated to the solution of the extended optimization problem by means of the interior-point method. Subsequently, a numerical example is investigated in Section 5, leading to the first representation of a three-dimensional shakedown domain accounting for kinematical hardening. After a detailed discussion of the results, the paper closes with concluding remarks and an outlook.

2 Lower bound shakedown analysis for elastic-perfectly plastic materials

An elastic-perfectly plastic body $\mathcal{K}$ with volume V and surface A is considered, which is subjected to varying: body forces $\boldsymbol{f}_V(\boldsymbol{x},t)$ in V, surface loads $\boldsymbol{f}_A(\boldsymbol{x},t)$ on $A_f \subseteq A$, and temperature loads $T(\boldsymbol{x},t)$ in V. In the following, only time- and temperature-independent material behavior is accounted for, while material damage and geometrical nonlinearity are omitted. The existence of a convex yield function $f[\boldsymbol{\sigma}(\boldsymbol{x},t),\sigma_Y(\boldsymbol{x})]$ and the validity of the normality rule are assumed.

2.1 MELAN's statical shakedown theorem

The current formulation is based on the statical shakedown theorem by MELAN [4,5], which provides a lower bound to the shakedown loading factor α_{SD}. For this, the total stress $\boldsymbol{\sigma}(\boldsymbol{x},t)$ –in a point $\boldsymbol{x} \in V$ at time t– is decomposed into an elastic reference stress $\boldsymbol{\sigma}^E(\boldsymbol{x},t)$ and a residual stress $\boldsymbol{\rho}(\boldsymbol{x},t)$ induced by the evolution of plastic strains

$$\boldsymbol{\sigma}(\boldsymbol{x},t) = \boldsymbol{\sigma}^E(\boldsymbol{x},t) + \boldsymbol{\rho}(\boldsymbol{x},t) \ , \tag{1}$$

where $\boldsymbol{\sigma}^E(\boldsymbol{x},t)$ denotes the stress state, which would occur in a fictitious purely elastic reference body $\mathcal{K}^E$ under the same conditions as the original one. Both the elastic reference stresses and the residual stresses satisfy the equilibrium constraints as well as the statical boundary conditions (bc).

$$\text{equilibrium:} \qquad \boldsymbol{\nabla}\cdot\boldsymbol{\sigma}^E = -\boldsymbol{f}_V \qquad \boldsymbol{\nabla}\cdot\boldsymbol{\rho} = \boldsymbol{0} \qquad \text{in } V \tag{2}$$

$$\text{statical bc:} \qquad \boldsymbol{n}\cdot\boldsymbol{\sigma}^E = \boldsymbol{f}_A \qquad \boldsymbol{n}\cdot\boldsymbol{\rho} = \boldsymbol{0} \qquad \text{on } A_f \tag{3}$$

Then, MELAN's shakedown theorem can be formulated as follows:
If there exists a time-independent residual stress field $\bar{\boldsymbol{\rho}}(\boldsymbol{x})$, such that the yield condition is satisfied for any loading path in the considered loading domain at any time t and in any point $\boldsymbol{x}$ of the structure, then the system will shake down.

$$f\left[\boldsymbol{\sigma}^E(\boldsymbol{x},t) + \bar{\boldsymbol{\rho}}(\boldsymbol{x}), \sigma_Y(\boldsymbol{x})\right] \leq 0, \ \forall \boldsymbol{x} \in V, \ \forall t \tag{4}$$

In the following, the loading domain is examined in order to deal with the time-dependence of $\boldsymbol{\sigma}^E(\boldsymbol{x}, t)$.

2.2 Description of the loading domain

It is assumed, that the loading histories $\mathcal{H}(\boldsymbol{x}, t)$ considered here can be described as superposition of finite numbers NL of different loading sets $P_\ell(\boldsymbol{x}, t)$. Then, scaling all loads by the load $P_0(\boldsymbol{x})$, load multipliers $\mu_\ell(t)$ can be introduced for any loading case ℓ reflecting the time-dependence of the loading.

$$\mathcal{H}(\boldsymbol{x}, t) = \sum_{\ell=1}^{NL} P_\ell(\boldsymbol{x}, t) = \sum_{\ell=1}^{NL} \mu_\ell(t)\, P_0(\boldsymbol{x}) \tag{5}$$

As shown by KÖNIG [8], it is sufficient to only consider the convex hull of the loading history. For this, the bounding values μ_ℓ^+ and μ_ℓ^- of each multiplier μ_ℓ are introduced. Thereby, the set $\mathcal{U}$ of all possible combinations of loading sets can be defined through merging all loading multipliers to the vector $\boldsymbol{\mu} = \mu_\ell\, \boldsymbol{e}_\ell$.

$$\mathcal{U} = \left\{ \boldsymbol{\mu} \in \mathbb{R}^{NL} \;\middle|\; \mu_\ell^- \leq \mu_\ell \leq \mu_\ell^+ \,,\, \forall \ell \in [1, NL] \right\} \tag{6}$$

Consequently, the loading domain Ω is described as set of all possible loading histories contained within this convex hull $\mathcal{U}$.

$$\Omega = \left\{ \mathcal{H}(\boldsymbol{x}, t) \;\middle|\; \mathcal{H}(\boldsymbol{x}, t) = \sum_{\ell=1}^{NL} \mu_\ell(t)\, P_0(\boldsymbol{x}) \,,\, \forall \boldsymbol{\mu} \in \mathcal{U} \right\} \tag{7}$$

As a result, the elastic reference stresses are split in analogy to (5).

$$\boldsymbol{\sigma}^E(\boldsymbol{x}, t) = \sum_{\ell=1}^{NL} \mu_\ell(t)\, \boldsymbol{\sigma}_\ell^E(\boldsymbol{x}) \tag{8}$$

2.3 Discretization

Using the finite element method (FEM), the stresses are approximately represented by their values in the Gaussian points, which will be referred to by the index $r \in [1, NG]$, where NG is the total number of Gaussian points in the system. Then, the fictitious elastic stresses $\boldsymbol{\sigma}_{r,\ell}^E$ can be computed for any loading case ℓ by purely elastic analysis.

$$\boldsymbol{\sigma}_r^E(t) = \sum_{\ell=1}^{NL} \mu_\ell(t)\, \boldsymbol{\sigma}_{r,\ell}^E \tag{9}$$

Since the loading domain Ω, which is spanned by the NL given loads, is polyhedral with $NC = 2^{NL}$ corners, it is sufficient to examine these corners only to ensure shake-down for all possible loading paths contained within Ω. Thus, the time-dependence

of $\boldsymbol{\sigma}_r^E(t)$ can be expressed through the stress states $\boldsymbol{\sigma}_r^{E,j}$ in the corners j of the loading domain. This is done by introducing the matrix $\boldsymbol{U}_{NL} \in \mathbb{R}^{NC\times NL}$ with entries $U_{j\ell}$ where $j \in [1, NC]$ and $\ell \in [1, NL]$. For details, the reader is referred to [44].

$$\boldsymbol{\sigma}_r^{E,j} = \sum_{\ell=1}^{NL} U_{j\ell}\boldsymbol{\sigma}_{r,\ell}^E \tag{10}$$

From (2) follows that the elastic reference stress field $\boldsymbol{\sigma}^E$ is in equilibrium with the external loading, whereas the residual stress field $\bar{\boldsymbol{\rho}}$ is self-equilibrated. This can be expressed using the principle of virtual work

$$\int_V \delta\boldsymbol{\varepsilon} : \bar{\boldsymbol{\rho}}\, dV = 0\,, \tag{11}$$

where $\delta\boldsymbol{\varepsilon}$ denotes any virtual strain field which satisfies the kinematical boundary conditions. Approximating the displacements $\boldsymbol{u}$ by appropriate shape functions and their nodal values $\boldsymbol{u}_K$, and introducing the differentiation matrix $\boldsymbol{B}(\boldsymbol{x})$, the strain field $\boldsymbol{\varepsilon}$ can be expressed as $\boldsymbol{\varepsilon} = \boldsymbol{B}(\boldsymbol{x}) \cdot \boldsymbol{u}_K$. Then, the principle of virtual work (11) reads

$$\int_V \delta\boldsymbol{\varepsilon} : \bar{\boldsymbol{\rho}}\, dV = \delta\boldsymbol{u}_K \cdot \int_V \boldsymbol{B}(\boldsymbol{x}) : \bar{\boldsymbol{\rho}}\, dV = 0 \quad \longrightarrow \quad \int_V \boldsymbol{B}(\boldsymbol{x}) : \bar{\boldsymbol{\rho}}\, dV = \boldsymbol{0} \tag{12}$$

This integration is carried out numerically, accounting for the necessary transition from the element-level to the system-level. Thereby, (11) is approximated by a system of linear equations for the residual stresses $\bar{\boldsymbol{\rho}}_r$ in the Gaussian points.

$$\int_V \boldsymbol{B}(\boldsymbol{x}) : \bar{\boldsymbol{\rho}}\, dV =: \sum_{r=1}^{NG} \mathbb{C}_r \cdot \bar{\boldsymbol{\rho}}_r = \boldsymbol{0} \tag{13}$$

The equilibrium matrices $\mathbb{C}_r \in \mathbb{R}^{m_E^*\times 6}$ depend only on the geometry of the system and the applied element type, and take into account the kinematical boundary conditions. Their dimension is $m_E^* = 3\,NK - NBC$, where NK is the total number of nodes and NBC the number of kinematical boundary conditions.

2.4 Resulting nonlinear optimization problem

Employing (10) and (13) and introducing the loading factor $\alpha > 1$, the statical shakedown theorem (4) can be formulated as optimization problem:

$$\begin{aligned}
(\mathcal{P}_{Melan}) \qquad & \alpha_{SD} = \max \alpha \\
& \sum_{r=1}^{NG} \mathbb{C}_r \cdot \bar{\boldsymbol{\rho}}_r = \boldsymbol{0} && \text{(14a)} \\
& \forall j \in [1, NC],\ \forall r \in [1, NG]: \\
& f\left(\alpha\, \boldsymbol{\sigma}_r^{E,j} + \bar{\boldsymbol{\rho}}_r, \sigma_{Y,r}\right) \le 0 && \text{(14b)}
\end{aligned}$$

3 Considering limited kinematical hardening

3.1 The two-surface model

In order to account for limited kinematical hardening, the two-surface model proposed by WEICHERT and GROSS-WEEGE [9] is used. Hence, kinematical hardening is considered as a translational movement of the yield surface without change of orientation, form or size. This movement is described in stress space by the six-dimensional vector of back-stresses $\boldsymbol{\pi}$, which represents the translation of the yield surface's center, see Fig. 1. The limitation of hardening is captured by introducing a second surfaces corresponding to the ultimate stress σ_H, which bounds the movement of the yield surface.

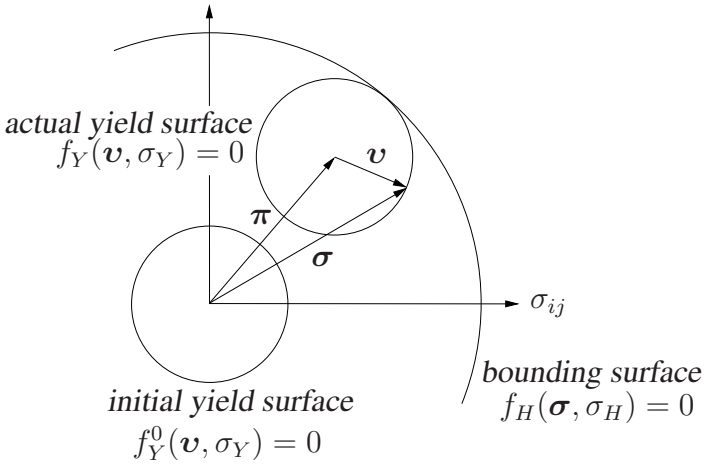

Figure 1: Kinematic hardening: Moving yield surface in stress space

Thereby, the total stresses are decomposed into the back-stresses $\boldsymbol{\pi}$ and the reduced stresses $\boldsymbol{\upsilon}$, which are responsible for the occurrence of plastic strains.

$$\boldsymbol{\sigma}(\boldsymbol{x}, t) = \boldsymbol{\pi}(\boldsymbol{x}, t) + \boldsymbol{\upsilon}(\boldsymbol{x}, t) \tag{15}$$

As before, the total stresses are divided as follows:

$$\boldsymbol{\sigma}_r^j = \alpha\, \boldsymbol{\sigma}_r^{E,j} + \bar{\boldsymbol{\rho}}_r \tag{16}$$

The reduced stresses $\boldsymbol{\upsilon}_r^j$ can be expressed analogously, keeping in mind that the back-stresses are time-independent, and thus independent of the considered corner j of the loading domain, because the bounding surface is fixed in stress space.

$$\boldsymbol{\upsilon}_r^j = \boldsymbol{\sigma}_r^j - \bar{\boldsymbol{\pi}}_r = \alpha\, \boldsymbol{\sigma}_r^{E,j} + \bar{\boldsymbol{\rho}}_r - \bar{\boldsymbol{\pi}}_r \tag{17}$$

Thereby, limited kinematical hardening is incorporated into the optimization problem:

$$
\begin{aligned}
(\mathcal{P}^{H}_{Melan}) \qquad & \alpha_{SD} = \max \alpha \\
& \sum_{r=1}^{NG} \mathbb{C}_r \cdot \bar{\boldsymbol{\rho}}_r = \mathbf{0} && \text{(18a)} \\
& \forall j \in [1, NC],\ \forall r \in [1, NG] : \\
& f_Y \left(\alpha\, \boldsymbol{\sigma}_r^{E,j} + \bar{\boldsymbol{\rho}}_r - \bar{\boldsymbol{\pi}}_r, \sigma_{Y,r} \right) \leq 0 && \text{(18b)} \\
& f_H \left(\alpha\, \boldsymbol{\sigma}_r^{E,j} + \bar{\boldsymbol{\rho}}_r, \sigma_{H,r} \right) \leq 0 && \text{(18c)}
\end{aligned}
$$

3.2 Tailoring to von Mises criterion

Both the yield surface $f_Y(\boldsymbol{\upsilon}, \sigma_Y)$ as well as the bounding surface $f_H(\boldsymbol{\sigma}, \sigma_H)$ are described by the VON MISES criterion, which can be written as follows, using $\boldsymbol{\delta}$ and σ as placeholders.

$$f\left(\boldsymbol{\delta}, \sigma\right) = \left(\delta_1 - \delta_2\right)^2 + \left(\delta_2 - \delta_3\right)^2 + \left(\delta_3 - \delta_1\right)^2 + 6\left[\left(\delta_4\right)^2 + \left(\delta_5\right)^2 + \left(\delta_6\right)^2\right] - 2\,\sigma^2 \quad (19)$$

This criterion is reformulated, as proposed by AKOA et al. [36], where $\boldsymbol{L} \in \mathbb{R}^{5\times5}$ and $\bar{\boldsymbol{T}} \in \mathbb{R}^{5\times6}$ are constant transformation matrices.

$$f\left(\boldsymbol{d}, \sigma\right) = \|\boldsymbol{d}\|_2^2 - 2\,\sigma^2 \qquad \text{where:} \qquad \boldsymbol{d} = \boldsymbol{L}^T \cdot \bar{\boldsymbol{T}}^{-1} \cdot \boldsymbol{\delta} \quad (20)$$

It should be noticed that this mathematical transformation from the six-dimensional vector $\boldsymbol{\delta}$ to the five-dimensional one $\boldsymbol{d}$ is also justified from physical point of view: the extracted component $\mathbf{v}$ represents the hydrostatic pressure, and thus has no influence on the VON MISES criterion. Accordingly, the yield and the bounding condition are achieved by substituting $\boldsymbol{\sigma}_r^j$ and $\boldsymbol{\upsilon}_r^j$ for the placeholder $\boldsymbol{\delta}$, respectively.

$$f\left(\boldsymbol{u}_r^j, \sigma_H\right) = \left\|\boldsymbol{u}_r^j\right\|_2^2 - 2\,\sigma_H^2 \qquad \text{where:} \qquad \boldsymbol{u}_r^j = \boldsymbol{L}^T \cdot \bar{\boldsymbol{T}}^{-1} \cdot \boldsymbol{\sigma}_r^j \quad (21)$$

$$f\left(\boldsymbol{\nu}_r^j, \sigma_Y\right) = \left\|\boldsymbol{\nu}_r^j\right\|_2^2 - 2\,\sigma_Y^2 \qquad \text{where:} \qquad \boldsymbol{\nu}_r^j = \boldsymbol{L}^T \cdot \bar{\boldsymbol{T}}^{-1} \cdot \boldsymbol{\upsilon}_r^j \quad (22)$$

Likewise, the condition for the residual stresses (13) has to be transformed, which requires to express it in terms of $\boldsymbol{\sigma}_r^j$ and $\boldsymbol{\sigma}_r^{E,j}$:

$$\sum_{r=1}^{NG} \mathbb{C}_r \cdot \bar{\boldsymbol{\rho}}_r = \sum_{r=1}^{NG} \mathbb{C}_r \cdot \left(\boldsymbol{\sigma}_r^j - \alpha \boldsymbol{\sigma}_r^{E,j}\right) = \mathbf{0} \quad (23)$$

Thereby, the information gets lost that the residual stresses are time-independent, implicating that $\bar{\boldsymbol{\rho}}$ does not depend on the considered corner j of the loading domain.

$$\bar{\boldsymbol{\rho}}_r = \boldsymbol{\sigma}_r^j - \alpha \boldsymbol{\sigma}_r^{E,j} = const(j) \quad (24)$$

Hence, this information has to be reintroduced to the problem as an additional constraint. Since (24) holds for all $j \in [1, NC]$, it can be used to link the stresses of

different corners of the loading domain with each other. In particular, considering the corners j and $j+1$, the following relation can be derived:

$$\boldsymbol{\sigma}_r^{j+1} - \alpha\boldsymbol{\sigma}_r^{E,j+1} = \bar{\boldsymbol{\rho}}_r \;=\; \boldsymbol{\sigma}_r^{j} - \alpha\boldsymbol{\sigma}_r^{E,j} \tag{25a}$$

$$\longrightarrow \qquad \boldsymbol{\sigma}_r^{j+1} = \boldsymbol{\sigma}_r^{j} - \alpha\left(\boldsymbol{\sigma}_r^{E,j} - \boldsymbol{\sigma}_r^{E,j+1}\right) \tag{25b}$$

Recalling (21), this leads to the following additional constraint for $\boldsymbol{u}_r^j$:

$$\boldsymbol{u}_r^{j+1} = \boldsymbol{u}_r^{j} - \alpha\,\boldsymbol{\gamma}_r^{j} \qquad \text{where:} \quad \boldsymbol{\gamma}_r^{j} = \boldsymbol{L}^T \cdot \bar{\boldsymbol{T}}^{-1} \cdot \left(\boldsymbol{\sigma}_r^{E,j} - \boldsymbol{\sigma}_r^{E,j+1}\right) \tag{26}$$

In the same manner, an additional constraint for the variables $\boldsymbol{\nu}_r^j$ is formulated, representing the fact that the back-stresses $\bar{\boldsymbol{\pi}}_r$ are time-independent.

$$\boldsymbol{\nu}_r^{j+1} = \boldsymbol{\nu}_r^{j} - \alpha\,\boldsymbol{\gamma}_r^{j} \tag{27}$$

In summary, the equality constraints (18a) –forcing the residual stresses to be self-equilibrated– are transformed to (23) together with the additional constraints

$$\boldsymbol{u}_r^{j+1} = \boldsymbol{u}_r^{j} - \alpha\,\boldsymbol{\gamma}_r^{j} \tag{28a}$$

$$\boldsymbol{\nu}_r^{j+1} = \boldsymbol{\nu}_r^{j} - \alpha\,\boldsymbol{\gamma}_r^{j}\;, \tag{28b}$$

while the inequality constraints (18b) and (18c) –representing the yield and the bounding surface– are expressed by

$$f\left(\boldsymbol{u}_r^j, \sigma_H\right) = \left\|\boldsymbol{u}_r^j\right\|_2^2 - 2\,\sigma_{H,r}^2 \leq 0 \tag{28c}$$

$$f\left(\boldsymbol{\nu}_r^j, \sigma_Y\right) = \left\|\boldsymbol{\nu}_r^j\right\|_2^2 - 2\,\sigma_{Y,r}^2 \leq 0\,. \tag{28d}$$

4 Solving the problem by the interior-point method

For the purpose of a clear presentation, the problem is rewritten more concisely:

$$(\mathcal{P}_{IP}^H) \qquad \min f(\boldsymbol{x}) = -\alpha$$

$$\boldsymbol{A}_H \cdot \boldsymbol{x} = \boldsymbol{0} \tag{29a}$$

$$\boldsymbol{c}_H(\boldsymbol{x}) = 2\,\sigma_{H,r}^2 - \left\|\boldsymbol{u}_r^j\right\|_2^2 \geq \boldsymbol{0} \tag{29b}$$

$$\boldsymbol{c}_Y(\boldsymbol{x}) = 2\,\sigma_{Y,r}^2 - \left\|\boldsymbol{\nu}_r^j\right\|_2^2 \geq \boldsymbol{0} \tag{29c}$$

$$\boldsymbol{x} \in \mathbb{R}^n\;, \tag{29d}$$

Here, the variables of the problem are merged to the solution vector

$$\boldsymbol{x} = \left[\boldsymbol{u}_1^1, \boldsymbol{u}_2^1, \ldots, \boldsymbol{u}_r^j, \ldots, \boldsymbol{u}_{NG}^{NC}, \boldsymbol{\nu}_1^1, \boldsymbol{\nu}_2^1, \ldots, \boldsymbol{\nu}_r^j, \ldots, \boldsymbol{\nu}_{NG}^{NC}, \mathbf{v}, \alpha\right]^T \in \mathbb{R}^n \tag{30}$$

of dimension n. This problem $(\mathcal{P}_{IP}^H)$ consists of m_E equality constraints, represented by the affine linear system of equations (29a), and $2\,m_I$ nonlinear concave inequality

constraints (29b) and (29c), where

$$n = 10\,NC \cdot NG + NG + 1 \tag{31}$$
$$m_E = m_E^* + 10NG \cdot (NC - 1) \tag{32}$$
$$m_I = NC \cdot NG\,. \tag{33}$$

The inequality constraints are converted into equality constraints by introducing slack variables $\boldsymbol{w}_H \in \mathbb{R}^{m_I}$ and $\boldsymbol{w}_Y \in \mathbb{R}^{m_I}$. Moreover, split variables $\boldsymbol{y} \in \mathbb{R}^n$ and $\boldsymbol{z} \in \mathbb{R}^n$ are used to avoid numerical instabilities due to the unboundedness of the solution vector (29d). Finally –as a key idea of the interior-point method– the objective function is perturbed by logarithmic barrier terms, which penalize directions leading outside of the feasible region. Thereby, the barrier parameter μ is introduced, which is a sequence tending to zero during the iteration.

$$\begin{aligned} f_\mu(\boldsymbol{x}, \boldsymbol{y}, \boldsymbol{z}, \boldsymbol{w}_H, \boldsymbol{w}_Y) &= f(\boldsymbol{x}) \\ &\quad - \mu \left[\sum_{i=1}^{n} \log(y_i) + \sum_{i=1}^{n} \log(z_i) + \sum_{j=1}^{m_I} \log(w_{H,j}) + \sum_{j=1}^{m_I} \log(w_{Y,j}) \right] \end{aligned} \tag{34}$$

The resulting optimization problem can be expressed as follows:

$$\begin{aligned} (\mathcal{P}_\mu^H) \qquad & \min f_\mu(\boldsymbol{x}, \boldsymbol{y}, \boldsymbol{z}, \boldsymbol{w}_H, \boldsymbol{w}_Y) \\ & \boldsymbol{A}_H \cdot \boldsymbol{x} = \boldsymbol{0} && \text{(35a)} \\ & \boldsymbol{c}_H(\boldsymbol{x}) - \boldsymbol{w}_H = \boldsymbol{0} && \text{(35b)} \\ & \boldsymbol{c}_Y(\boldsymbol{x}) - \boldsymbol{w}_Y = \boldsymbol{0} && \text{(35c)} \\ & \boldsymbol{x} - \boldsymbol{y} + \boldsymbol{z} = \boldsymbol{0} && \text{(35d)} \\ & \boldsymbol{w}_H > \boldsymbol{0},\ \boldsymbol{w}_Y > \boldsymbol{0},\ \boldsymbol{y} > \boldsymbol{0},\ \boldsymbol{z} > \boldsymbol{0} && \text{(35e)} \end{aligned}$$

As already mentioned, this optimization problem is convex and regular. For such problems, the Karush-Kuhn-Tucker condition is both necessary and sufficient, which states that the solution is optimal if the Lagrangian of the problem possesses a saddle point. Considering $(\mathcal{P}_\mu^H)$, the Lagrangian $\mathcal{L}_H$ is expressed by

$$\begin{aligned} \mathcal{L}_H = f_\mu(\boldsymbol{x}, \boldsymbol{y}, \boldsymbol{z}, \boldsymbol{w}_H, \boldsymbol{w}_Y) &- \boldsymbol{\lambda}_H \cdot (\boldsymbol{c}_H(\boldsymbol{x}) - \boldsymbol{w}_H) - \boldsymbol{\lambda}_Y \cdot (\boldsymbol{c}_Y(\boldsymbol{x}) - \boldsymbol{w}_Y) \\ &- \boldsymbol{\lambda}_E \cdot (\boldsymbol{A}_H \cdot \boldsymbol{x}) - \boldsymbol{s} \cdot (\boldsymbol{x} - \boldsymbol{y} + \boldsymbol{z})\,, \end{aligned} \tag{36}$$

where $\boldsymbol{\lambda}_E \in \mathbb{R}^{m_E}$, $\boldsymbol{\lambda}_H \in \mathbb{R}_+^{m_I}$, $\boldsymbol{\lambda}_Y \in \mathbb{R}_+^{m_I}$ and $\boldsymbol{s} \in \mathbb{R}_+^n$ are appropriate Lagrange multipliers. Then, the saddle point condition can be evaluated as

$$\boldsymbol{\nabla}_{\Pi} \mathcal{L}_H(\boldsymbol{\Pi}) = \boldsymbol{0} \tag{37}$$

Here, $\boldsymbol{\Pi} = [\boldsymbol{x}, \boldsymbol{y}, \boldsymbol{z}, \boldsymbol{w}_H, \boldsymbol{w}_Y, \boldsymbol{\lambda}_E, \boldsymbol{\lambda}_H, \boldsymbol{\lambda}_Y, \boldsymbol{s}]^T$ denotes the vector of all variables included in this problem.

Equation (37) constitutes a system of nonlinear equations, which is solved approximately by use of the Newton's method. The variables $\boldsymbol{\Pi}_{k+1}$ of the subsequent iteration step $k+1$ are computed from the variables $\boldsymbol{\Pi}_k$ of the previous one k and the step values $\Delta\boldsymbol{\Pi}_k$.

$$\boldsymbol{\Pi}_{k+1} = \boldsymbol{\Pi}_k + \Upsilon_k \, \Delta\boldsymbol{\Pi}_k \ , \tag{38}$$

Noteworthy, the diagonal matrix Υ_k of damping factors is introduced to guarantee convergence of the iterative procedure. In consequence, the step values $\Delta\boldsymbol{\Pi}_k$ are determined from the following linearized system of equations.

$$\boldsymbol{J}(\boldsymbol{\Pi}_k) \cdot \Delta\boldsymbol{\Pi}_k = -\boldsymbol{\nabla}_{\Pi}\mathcal{L}_H(\boldsymbol{\Pi}_k) \tag{39}$$

$$\text{where:} \qquad \boldsymbol{J}(\boldsymbol{\Pi}_k) = \boldsymbol{\nabla}_{\Pi}\mathcal{L}_H(\boldsymbol{\Pi})\,\boldsymbol{\nabla}_{\Pi}\Big|_{\boldsymbol{\Pi}=\boldsymbol{\Pi}_k}$$

In each iteration step, the Jacobian $\boldsymbol{J}(\boldsymbol{\Pi}_k)$ is build and the linearized system of equations (39) is solved for the step values $\Delta\boldsymbol{\Pi}_k$. Then, an inner loop is applied to ensure that this solution is sufficiently accurate for the original nonlinear system. In case of negative components in the slack variables, the split variables, or the Lagrange multipliers of the inequality constraints, the computed step is damped to satisfy the non-negativity conditions. Notably, further damping may be necessary, which is performed by means of a linesearch procedure using the ℓ_2-merit function. Once the damped step values are computed, the new variables can be easily determined from (38). Subsequently, the break condition is checked based on appropriate convergence criteria. If the solution is not yet converged, the barrier parameter μ is decreased and the next iteration step is entered. For further descriptions of the numerical procedure, the reader is referred to [41].

5 Numerical example

The proposed method was applied to a flanged pipe with three different outer radii, see Fig. 2(a), already considered by MOUHTAMID [45] and WEICHERT et al. [46]. Both the dimensions as well as the material data were adopted from [45], see Tab. 1 and Tab. 2. The FEM-analysis was carried out with the software package ANSYS using the isoparametric hexahedral solid element *solid45*. Taking advantage of the system's rotational symmetry –as shown in Fig. 2(b)– the applied mesh consisted of 265 elements and 678 nodes, where one element across the thickness was used.

5.1 Two-dimensional loading space

To validate the method, the system was first investigated in a two-dimensional loading space. In particular, the pipe was subjected to an internal pressure p and an axial force Q, which varied independently in the ranges $p \in [0; p_{max}]$ and $Q \in [0; Q_{max}]$, respectively.

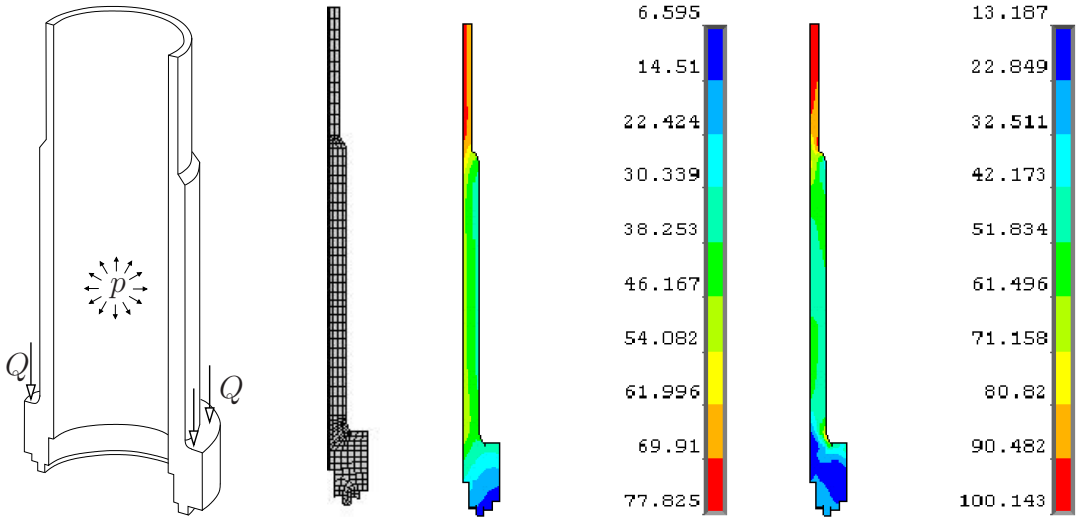

(a) System and loading (b) Model (c) Equivalent elastic stresses due to pressure (d) Equivalent elastic stresses due to axial force

Figure 2: System, model and equivalent elastic stresses for the flanged pipe

Length L	386.9
Inner radius R_i	60.0
Outer radius $R_{a,1}$	68.1
Outer radius $R_{a,2}$	77.8
Outer radius $R_{a,3}$	90.5

Table 1: Dimensions in mm

Young's modulus [MPa]	2.0×10^5
Yield stress [MPa]	200
Poisson's ratio	0.3
Density [kg/m^3]	7.9×10^3
Thermal conductivity [W/(m·K)]	15
Specific heat capacity [J/(kg·K)]	500
Coefficient of thermal expansion [1/K]	1.6×10^{-5}

Table 2: Thermal and mechanical characteristics

In order to compute the elastic stresses presented in Fig. 2(c) and Fig. 2(d), the arbitrary values $p = 10$ MPa and $Q = 113.097$ kN were applied, respectively.

As a result of the shakedown analysis, Fig. 3 presents: the elastic domain and twice the elastic domain (dotted lines); the shakedown domains without consideration of hardening for the yield stress $\sigma_Y = 200$ MPa (solid line), and for multiples of the yield stress $\sigma^*_{Y,1} = 1.25\,\sigma_Y$ and $\sigma^*_{Y,2} = 1.5\,\sigma_Y$ (dash-dot lines); the shakedown domains including hardening with different values of ultimate stresses $\sigma_{H,1} = 1.25\,\sigma_Y$ and $\sigma_{H,2} = 1.5\,\sigma_Y$ (solid lines); the shakedown domain with unlimited kinematical hardening (solid line). Both axes are scaled to the according value p_0 and Q_0, respectively, for perfectly plastic material behavior.

In all cases –both the perfectly plastic and the hardening one– the two mechanisms of alternating plasticity and incremental collapse can be clearly distinguished:
In case of predominating axial force, all shakedown curves coincide with the one for unlimited hardening, indicating that alternating plasticity is decisive here. Hence, no influence of hardening can be observed.

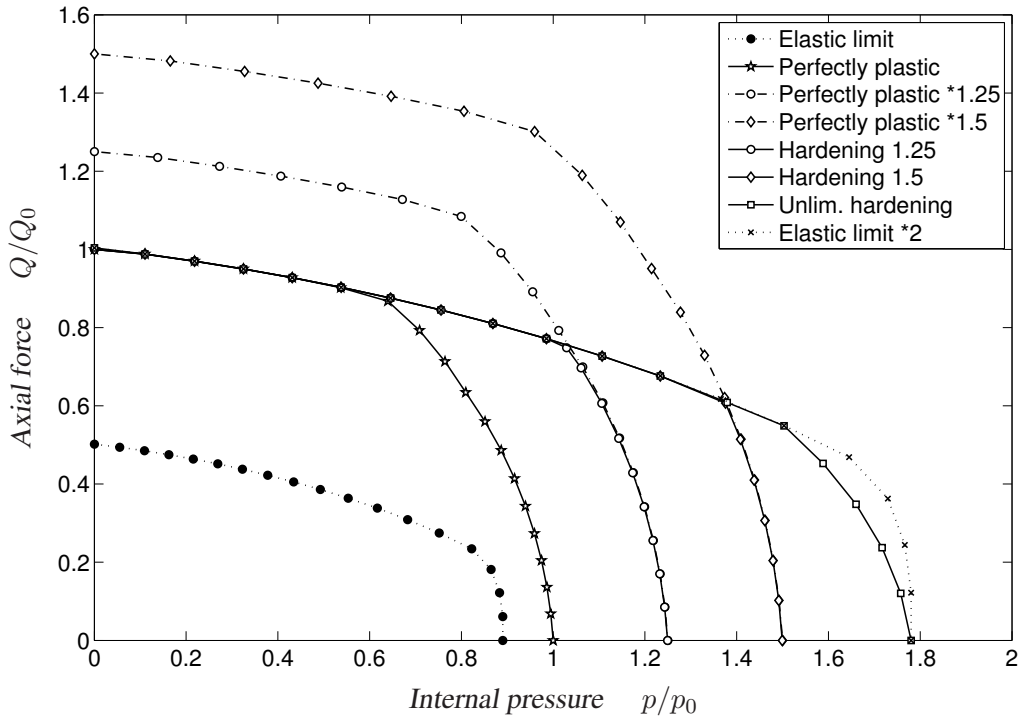

Figure 3: Results of shakedown analysis of the flanged pipe

By contrast, failure is due to incremental collapse in the regime of predominating internal pressure, where the limited kinematical hardening leads to an increase of the according shakedown domains in direct proportion with the ratio σ_H/σ_Y. Thus, the hardening curves (solid lines) coincide with the corresponding none-hardening ones with premultiplied yield stress (dash-dot lines) in this range.
In all cases, the two curves pass into each other seamlessly.

It should be noticed, that the unlimited hardening curve does only accord partly with double the elastic domain. Even so, it is frequently stated in the literature, that these curves have to accord in the whole domain, which simply is wrong. In fact, they have to coincide only at the axis intercepts. In the remaining domain, they may –but do not must– be the same.

For validation, in Fig. 4 the results obtained by the new method are compared to those reported in [45], which have been computed on the basis of the augmented Lagrangian method using the program LANCELOT [47]. In general, matching of the results is satisfying, especially for limited kinematical hardening with $\sigma_H = 1.5\,\sigma_Y$. However, slight differences exist resulting from different elastic solutions. These can be explained by the use of different meshes. In particular, the maximum equivalent stress under axial force is 106.465 MPa in [45], whereas the current calculation yields 100.143 MPa.

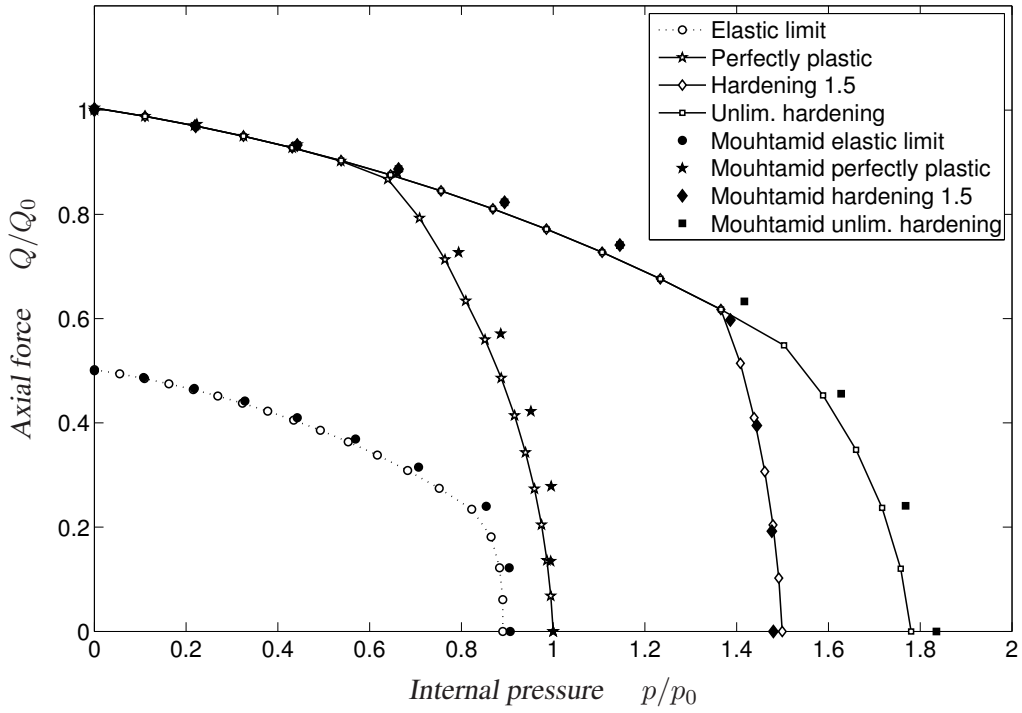

Figure 4: Comparison with results from MOUHTAMID [45]

5.2 Three-dimensional loading space

To illustrate the influence of hardening in a three-dimensional loading space, a temperature load $\Delta T \in [0; \Delta T_{max}]$ was applied additionally. The according FEM-analysis was carried out in two steps: (1) using the hexahedral thermal element *solid70*, the body temperature distribution was computed resulting from prescribed temperature bounding conditions of $T_i = 100$ K and $T_o = 20$ K at the inner and the outer surface of the pipe, respectively, see Fig. 5(a); (2) based on the body temperature distribution, nodal temperature loadings were defined for the structural analysis with element *solid45*, leading to the equivalent elastic stress distribution shown in Fig. 5(b).

Noteworthy, in the whole calculation, all material parameters were assumed to be temperature-independent. Furthermore, only steady-state processes were considered.

Applying the proposed algorithm, the three-dimensional shakedown domain was computed for elastic-perfectly plastic material, see Fig. 6. Further, the influence of limited kinematical hardening was investigated by calculations with different ultimate stresses: $\sigma_H = 1.1\,\sigma_Y$ (Fig. 7 and blue dash-dot line), $\sigma_H = 1.25\,\sigma_Y$ (Fig. 8 and blue dashed line), and $\sigma_H = 1.5\,\sigma_Y$ (Fig. 9 and black dash-dot line). Subsequently, the domain was determined for unlimited hardening (Fig. 10 and black solid line).

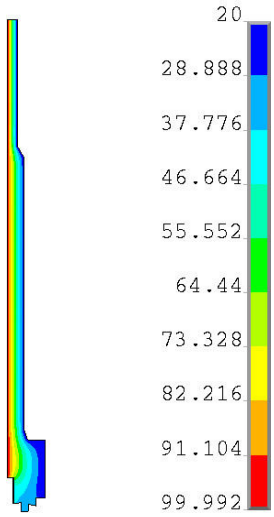

(a) Distribution of body temperature

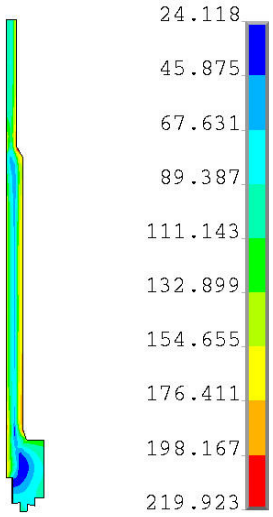

(b) Equivalent elastic stresses due to temperature loading

Figure 5: Body temperature distribution and resulting equivalent elastic stresses

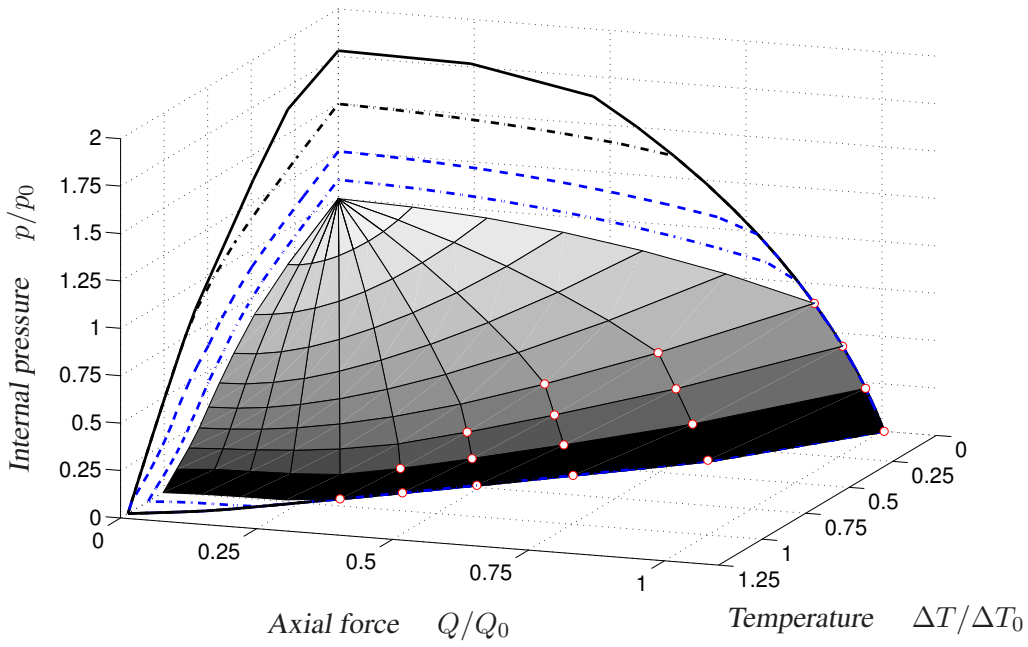

Figure 6: Three-dimensional shakedown domain without hardening

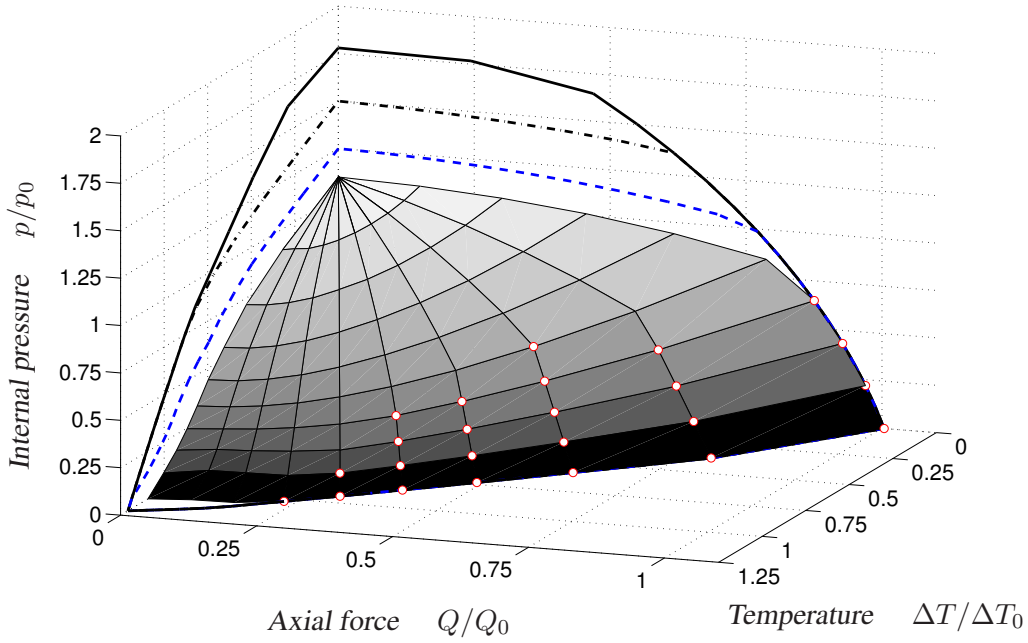

Figure 7: Three-dimensional shakedown domain with hardening $\sigma_H = 1.1\,\sigma_Y$

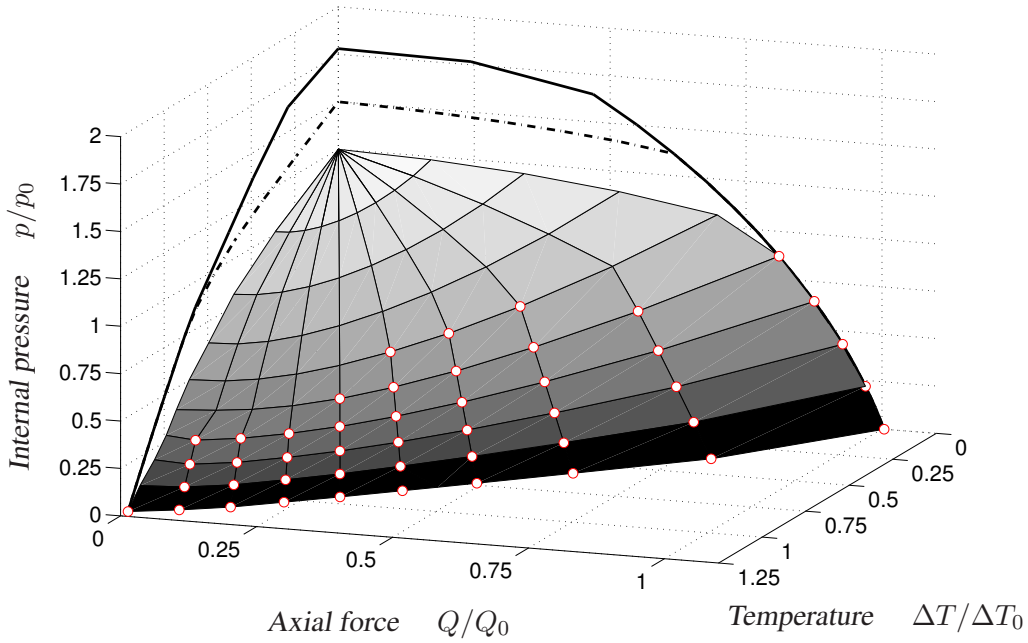

Figure 8: Three-dimensional shakedown domain with hardening $\sigma_H = 1.25\,\sigma_Y$

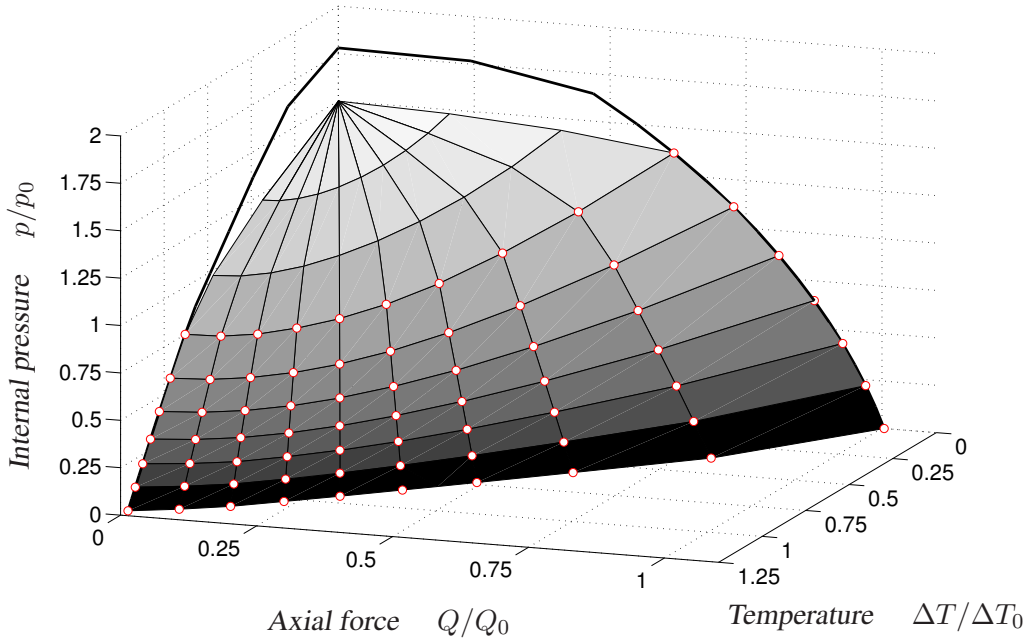

Figure 9: Three-dimensional shakedown domain with hardening $\sigma_H = 1.5\,\sigma_Y$

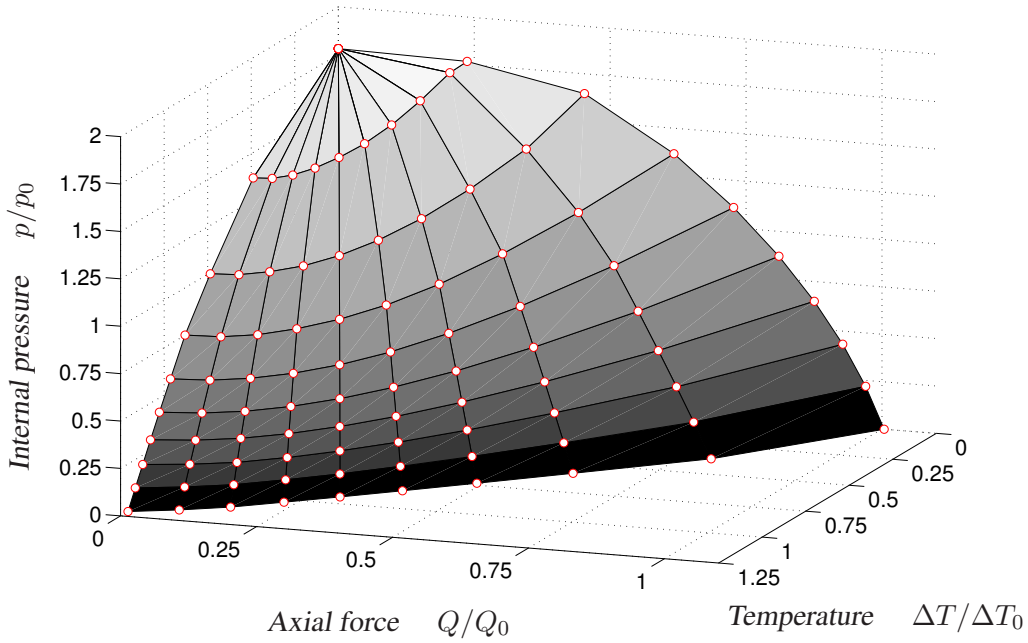

Figure 10: Three-dimensional shakedown domain with unlimited hardening

As in the two-dimensional case, the two mechanisms alternating plasticity and incremental collapse can be clearly distinguished. To highlight this, all computed points leading to alternating plasticity are marked by red circles.

In the regime of predominating temperature, all shakedown domains coincide, which implicates alternating plasticity to be decisive. Here, hardening does not affect the solution. By contrast, an influence of hardening can be observed in the regime of predominating axial force. While incremental collapse leads to failure in the elastic-perfectly plastic case as well as when considering limited hardening with $\sigma_H = 1.1\,\sigma_Y$, further increasing the ultimate stress has no impact, because alternating plasticity occurs starting from $\sigma_H = 1.2\,\sigma_Y$. Finally, when the internal pressure is superior, hardening enlarges the shakedown domain in direct proportion with the ratio σ_H/σ_Y in all calculations with limited hardening. Only for unlimited hardening, its effect its restricted and alternating plasticity appears.

Closing, the characteristic numerical details are reported in Tab. 3. As one can see, the number of iterations is not as much affected as the running time. Moreover, in the considered example, the number of loadings has a larger impact than the hardening, even though the numbers of variables and constraints are comparable.

	2 independent loads		3 independent loads	
	Perfectly plastic	Hardening	Perfectly plastic	Hardening
n	44 521	86 921	86 921	171 721
m_E	33 834	65 634	76 234	150 434
m_I	8 480	16 960	16 960	33 920
∅ Iterations	400	481	2 318	3 017
∅ CPU-time [s] *	48	57	295	837

* *Dell Precision T7500* with *Xeon E5620*-processor with 2400 MHz and 12 GB RAM

Table 3: Influence of hardening on numerical details

6 Conclusions

Evaluating the limit states of elasto-plastic engineering structures is essential for their design. To realistically predict the according shakedown loading domains, incorporating limited kinematical hardening is inevitable. On the other hand, complex loading situations arise in most technical applications, which cannot be reflected by only two-dimensional loading spaces. Thus, shakedown analysis can only be applied expediently to realistic engineering problems of practical relevance, if both limited kinematical hardening and complex loadings can be dealt with at the same time. Since, as yet, no tools with this capability have been available, the method has been restricted to special cases only, confining its operational area to academic problems mainly. The

new approach presented in this paper eradicates these restrictions and thus exhibits the potential to overcome the gap between academic research and practical application.

References

[1] D. Weichert, G. Maier, *Inelastic analysis of structures under variable repeated loads*, Kluwer Academic Publishers, Dordrecht, 2000.

[2] G. Maier, J. Pastor, A. Ponter, D. Weichert, "Direct methods of limit and shakedown analysis", in R. de Borst, H. Mang (Editors), *Comprehensive Structural Integrity – Fracture of Materials from Nano to Macro*, Volume 3: Numerical and Computational Methods, pages 637–684. Elsevier, 2003.

[3] D. Weichert, A. Ponter, *Limit states of materials and structures*, Springer, Wien/New York, 2009.

[4] E. Melan, "Der Spannungszustand eines "Mises-Hencky'schen" Kontinuums bei veränderlicher Belastung", *Sitzungsber Akad Wiss Wien, math-nat Kl, Abt IIa*, 147: 73–87, 1938.

[5] E. Melan, "Zur Plastizität des räumlichen Kontinuums", *Ing-Arch*, 9: 116–126, 1938.

[6] A. Ponter, "A general shakedown theorem for elastic plastic bodies with work hardening", in *Proc SMIRT–3, paper L5/2*, 1975.

[7] J. Zarka, J. Casier, "Elastic-plastic response of a structure to cyclic loading: practical rule", in S. Nemat-Nasser (Editor), *Mechanics today*, Volume 6. Pergamon, 1981.

[8] J. König, *Shakedown of elastic-plastic structures*, Elsevier, Amsterdam, 1987.

[9] D. Weichert, J. Groß-Weege, "The numerical assessment of elastic-plastic sheets under variable mechanical and thermal loads using a simplified two-surface yield condition", *Int J Mech Sci*, 30(10): 757–767, 1988.

[10] J. Groß-Weege, D. Weichert, "Elastic-plastic shells under variable mechanical and thermal loads", *Int J Mech Sci*, 34: 863–880, 1992.

[11] E. Stein, G. Zhang, J. König, "Shakedown with nonlinear strain-hardening including structural computation using finite element method", *Int J Plast*, 8(1): 1–31, 1992.

[12] E. Stein, G. Zhang, Y. Huang, "Modeling and computation of shakedown problems for nonlinear hardening materials", *Comput Methods Appl Mech Engrg*, 103(1–2): 247–272, 1993.

[13] M. Heitzer, *Traglast- und Einspielanalyse zur Bewertung der Sicherheit passiver Komponenten*, PhD thesis, Forschungszentrum Jülich, RWTH Aachen, Germany, 1999.

[14] M. Staat, M. Heitzer, "The restricted influence of kinematical hardening on shakedown loads", in *Proc WCCM V*, 2002.

[15] Q.S. Nguyen, "On shakedown analysis in hardening plasticity", *J Mech Phys Solids*, 51: 101–125, 2003.

[16] P. Pham, D. Vu, T. Tran, M. Staat, "An upper bound algorithm for shakedown

analysis of elastic-plastic bounded linearly kinematic hardening bodies", in *Proc ECCM 2010*, 2010.

[17] A. Forsgren, P. Gill, M. Wright, "Interior methods for nonlinear optimization", *SIAM Rev*, 44(4): 525–597, 2002.

[18] M. Wright, "The interior-point revolution in optimization: History, recent developments and lasting consequences", *Bull Amer Math Soc*, 42(1): 39–56, 2004.

[19] A. Wächter, L. Biegler, "Line-search filter methods for nonlinear programming: Motivation and global convergence", *SIAM J Optim*, 16(1): 1–31, 2005.

[20] A. Wächter, L. Biegler, "On the implementation of an interior-point filter line-search algorithm for large-scale nonlinear programming", *Math Program*, 106 (1): 25–57, 2006.

[21] R. Byrd, M. Hribar, J. Nocedal, "An interior point algorithm for large-scale nonlinear programming", *SIAM J Optim*, 9(4): 877–900, 2000.

[22] R. Waltz, J. Morales, J. Nocedal, D. Orban, "An interior algorithm for nonlinear optimization that combines line search and trust region steps", *Math Program*, 107(3): 391–408, 2006.

[23] R. Vanderbei, "LOQO: An interior point code for quadratic programming", *Optim Meth & Soft*, 11–12: 451–484, 1999.

[24] I. Griva, D. Shanno, R. Vanderbei, H. Benson, "Global convergence analysis of a primal-dual interior-point method for nonlinear programming", *Algorithm Oper Res*, 3(1): 12–19, 2008.

[25] E. Andersen, C. Roos, T. Terlaky, "On implementing a primal-dual interior-point method for conic quadratic optimization", *Math Program*, 95(2): 249–277, 2003.

[26] E. Andersen, B. Jensen, J. Jensen, R. Sandvik, U. Worsøe, "MOSEK version 6", Technical Report TR–2009–3, MOSEK, 2009.

[27] C. Bisbos, A. Makrodimopoulos, P. Pardalos, "Second-order cone programming approaches to static shakedown analysis in steel plasticity", *Optim Meth & Soft*, 20(1): 25–52, 2005.

[28] A. Makrodimopoulos, "Computational formulation of shakedown analysis as a conic quadratic optimization problem", *Mech Res Commun*, 33: 72–83, 2006.

[29] K. Krabbenhøft, A. Lyamin, S. Sloan, "Formulation and solution of some plasticity problems as conic programs", *Int J Solids Struct*, 44: 1533–1549, 2007.

[30] F. Pastor, P. Thoré, E. Loute, J. Pastor, M. Trillat, "Convex optimization and limit analysis: Application to Gurson and porous Drucker-Prager materials", *Eng Fract Mech*, 75: 1367–1383, 2008.

[31] N. Zouain, L. Borges, J. Silveira, "An algorithm for shakedown analysis with nonlinear yield functions", *Comput Methods Appl Mech Engrg*, 191: 2463–2481, 2002.

[32] A. Lyamin, S. Sloan, "Lower bound limit analysis using nonlinear programing", *Int J Numer Methods Engng*, 55: 573–611, 2002.

[33] K. Krabbenhøft, L. Damkilde, "A general nonlinear optimization algorithm for lower bound limit analysis", *Int J Numer Methods Engng*, 56: 165–184, 2003.

[34] D. Vu, A. Yan, H. Nguyen-Dang, "A dual form for discretized kinematic formu-

lation in shakedown analysis", *Int J Solids Struct*, 41: 267–277, 2004.
[35] A. Hachemi, S. Mouhtamid, D. Weichert, "Progress in shakedown analysis with applications to composites", *Arch Appl Mech*, 74: 762–772, 2005.
[36] F. Akoa, A. Hachemi, H.A. Le Thi, S. Mouhtamid, T. Pham Dinh, "Application of lower bound direct method to engineering structures", *J Glob Optim*, 37(4): 609–630, 2007.
[37] K. Krabbenhøft, A. Lyamin, S. Sloan, P. Wriggers, "An interior-point algorithm for elastoplasticity", *Int J Numer Methods Engng*, 69: 592–626, 2007.
[38] D. Vu, M. Staat, "Analysis of pressure equipment by application of the primal-dual theory of shakedown", *Comm Numer Methods Engng*, 23(3): 213–225, 2007.
[39] F. Pastor, E. Loute, J. Pastor, M. Trillat, "Mixed method and convex optimization for limit analysis of homogeneous Gurson materials: a kinematic approach", *Eur J Mech A/Solids*, 28: 25–35, 2009.
[40] F. Pastor, E. Loute, "Limit analysis decomposition and finite element mixed method", *J Comput Appl Math*, 234(7): 2213–2221, 2010.
[41] J.W. Simon, D. Weichert, "Numerical Lower Bound Shakedown Analysis of Engineering Structures", *Comput Methods Appl Mech Engrg*, 200: 2828–2839, 2011.
[42] J.W. Simon, M. Chen, D. Weichert, "Shakedown analysis combined with the problem of heat conduction", *J Pressure Vessel Technol*, 134(2): 021206/1–8, 2012.
[43] J.W. Simon, D. Weichert, "Interior-point method for shakedown analysis accounting for limited kinematic hardening", in *Conf Proc COMPLAS2011*, 2011.
[44] J.W. Simon, D. Weichert, "Shakedown analysis with multidimensional loading spaces", *Comput Mech*, 49(4): 477–485, 2012.
[45] S. Mouhtamid, *Anwendung direkter Methoden zur industriellen Berechnung von Grenzlasten mechanischer Komponenten*, PhD thesis, Institute of General Mechanics, RWTH Aachen University, Germany, 2007.
[46] D. Weichert, A. Hachemi, S. Mouhtamid, A. Nguyen, "On recent progress in shakedown analysis and applications to large-scale problems", in *IUTAM Symposium on theoretical, computational and modelling aspects of inelastic media*, Volume 11, pages 349–359. 2008.
[47] A. Conn, N. Gould, P. Toint, *LANCELOT: a Fortran package for large-scale nonlinear optimization (Release A)*, Volume 17, Springer Series Comput Math, Heidelberg/New York, 1992.